Applied Thermal Engineering xxx (xxxx) xxx

Contents lists available at ScienceDirect

Applied Thermal Engineering

journal homepage: www.elsevier.com/locate/apthermeng

Research Paper

Bidirectional temperature control with thermochemical reactions

Hanna Lösch *, Eva Fensterle, Marc Linder, Inga Bürger

Institute of Engineering Thermodynamics, German Aerospace Center (DLR), Pfaffenwaldring 38-40, 70569 Stuttgart, Germany

ARTICLE INFO

Keywords:
Thermochemical energy storage
Operation strategy
Gas flow control
Metal hydride
Thermal capacitor
Temperature control
Hydrogen

ABSTRACT

Precise and reliable temperature control is crucial for many industrial processes and components. Common active temperature control systems require parasitic power while passive temperature control cannot be adjusted to different temperature set points and disturbances. A new approach is a temperature control based on a thermochemical thermal capacitor, which controls the temperature actively and does not use parasitic power, but potential energy to drive the process. In this study, such a thermal capacitor is introduced and investigated. The concept is based on a reversible thermochemical reaction which is characterized by a temperature pressure correlation, and thus enables the pressure as actuating variable. As exemplary material, $LaNi_5$ has been used. First, a 0D-model of the metal hydride reactor was developed and experimentally validated to optimize a PID controller for the thermochemical system. Resulting experiments with the thermal capacitor and controller prove the active and bidirectional temperature control of the system for temperature disturbances of 1.5 K. Additionally, the 0D-model was extended with an inverted 0D-model functioning as controller to show the characteristics of such a thermal capacitor using generic sinusoidal temperature disturbances. The simulative results indicate two major technical features of the presented system: the set temperature can easily be adjusted during operation and the dynamics of the thermal capacitor can be adapted to follow disturbances with various frequencies and amplitudes. Besides that, the underlying model presented in this work can be used for the improvement of thermochemical batch reactors under transient load as well as to optimize controllers and connecting reactors for applications.

1. Introduction

Industrial processes and technical components e.g. usage of waste heat and fuel cells benefit from or even require constant inlet temperatures of the working fluid. A constant inlet temperature of a working fluid leads to smaller components for the usage of waste heat [1,5–9] and a longer life cycle of fuel cells [10–12] to follow both examples. However, temperature peaks occur due to load changes in the processes. Therefore, technologies buffering temperature peaks are required. One option to address this problem would be an active cooling or heating of the system. However, this approach needs parasitic power and leads to inefficient use of thermal energy [13]. One prominent technology for efficient thermal energy usage are thermal energy storages, which are able to buffer energy from times with high offer and low demand and release the energy again at high demand and low offer events.

One of these currently investigated storage approaches are based on the implementation of phase change materials (PCM) to stabilize the system or process temperature and act as thermal energy storage. In this case, the PCM stores and releases the thermal energy at its intrinsic phase change temperature and is thus acting as so-called thermal capacitor. Due to this defined phase change temperature, a PCM based thermal capacitor can act as heat source and sink in the same process and provide both requirements with only few losses [14]. A disadvantage of a thermal energy storage compared to current temperature control systems is the limitation due to the storage capacity leading to batch effects, thus the storage capacity is one main design factor depending on the application [2,3,5,7,15,16].

Next to the PCM technology, thermochemical reactions have a huge potential to store thermal energy and stabilize temperatures when acting as a thermal capacitor. Similarly to the PCM systems, those kinds of reversible reactions also show the possibility to store and release heat at a distinct temperature [9,17]. However, in contrast to the PCM thermal capacitor, the thermochemical based approach can even adjust the specific reaction temperature: For gas solid based thermochemical reactions this is possible by simply adjusting the gas pressure [18]. Wild et. al [18] heated the HTF outlet temperature to a temperature set point during a constant inlet temperature with a closed thermochemical

* Corresponding author.
E-mail address: hanna.loesch@dlr.de (H. Lösch).

https://doi.org/10.1016/j.applthermaleng.2025.126681
Received 17 February 2025; Received in revised form 28 April 2025; Accepted 30 April 2025
Available online 1 May 2025

Nomenclature

λ	thermal conductivity (W m^{-1} K^{-1})
ρ_g	gas density (kg/m^3)
ρ_{HTF}	heat transfer fluid density (kg/m^3)
$c_{p/}c_v$	specific heat capacity (J kg^{-1} K^{-1})
$\Delta T_{MH,HTF}$	logarithmic average temperature between metal hydride and heat transfer fluid (K)
e_p	pressure difference to set point, outer control circuit (bar)
e_T	temperature difference to set point (K)
G_{th}	thermal conductance (W/K)
H	reaction enthalpy (J/mol)
K_{Ar}	Arrhenius coefficient (1/s)
K_P	gain factor of PID-controller
M_{H2}	molar mass from hydrogen (kg/mol)
m_{MH}	metal hydride mass (kg)
$\dot{m}_{H_2}$	hydrogen mass flow (kg/s)
$\dot{m}_{HTF}$	mass flow of heat transfer fluid (kg/s)
p_0	initial pressure (Pa)
p_{eq}	equilibrium pressure (Pa)
p_{gr}	reaction gas pressure (Pa)
p_{sp}	pressure set point (bar)
R	molar gas constant (J mol^{-1} K^{-1})
R^2	coefficient of determination (%)
S	reaction entropy (J mol^{-1} K^{-1})
T_1	delay time of PID-controller (s)
T_D	derivative time constant (s)
T_{HTF}	temperature of heat transfer fluid (K)
T_I	integration time constant of PID-controller (s)
T_{MH}	metal hydride temperature (K)
V_{HTF}	volume of the heat transfer fluid (m^3)
V_v	void volume (m^3)
x	hydrogen loading of metal hydride

Subscripts

in	inlet
out	outlet

Abbreviations

HTF	heat transfer fluid
IM	inverted simplified model
MH	metal hydride
PCM	Phase Change Material
PLC	programmable logic controller
SoC	state of charge

system by controlling the pressure of the energy storage. Gehring et. al [19] investigated a first open bidirectional temperature control system with a thermochemical reactor using metal hydrides (MH), which can be implemented in an hydrogen infrastructure [19]. The present paper follows these ideas but broadens the perspective in order to improve the stabilization capabilities and to investigate additional features and challenges of such thermochemical capacitors in a more generic approach. This paper will show directly the opportunities of a thermochemical capacitor and its ability to adjust to different disturbances by changing the pressure.

Thermochemical reactions are mostly used as energy storage systems and serve either as cooling or heating device [8,9]. Equation (1) defines generally a reversible thermochemical reaction of a solid (A, AB) with a gas (B), which is *ex*-or endothermal. This implies the possibility to heat or cool-depending on the temperature difference between the application and the reacting material.

$$A + B \leftrightarrows AB + \Delta H. \quad (1)$$

The intrinsic pressure and temperature dependence of this system and the resulting materials equilibrium can be described by the so called van't Hoff relation (compare also Fig. 2). If the operation pressure is above the equilibrium pressure for the operating temperature, the equilibrium is shifted to right of the Equation (1 and an exothermic absorption reaction takes place. If the operation pressure is below the equilibrium pressure, the system answers with the reverse endothermic desorption.

There are two specific features of this reaction which have a strong impact on the application as thermal capacitor. First, the reaction is limited by the capacity of the material and the amount of material, thus it refers to a batch process. For final applications, this characteristic has strong impact on the sizing of the system. Second, the reaction kinetics of this reversible reaction can be regulated by the reaction gas pressure. Generally speaking, "the further away", the operation point from the equilibrium point, the faster the reaction kinetics. This feature is specific for thermochemical systems and is a distinct advantage in comparison to PCM applications as it enables not only a bidirectional temperature stabilization – but actually allows to use the gas pressure as actuating variable and thereby actively control the thermal intensity.

One example of a thermochemical reaction system is the reaction between specific metals and hydrogen forming a metal hydride (MH). One significant advantage of such metal hydride systems is the possibility of an integration as thermal capacitor in every hydrogen system: The metal hydride can then take advantage of the pressure difference between the required pressure of the application, e.g. fuel cell and the supply pressure of the tank. Thus, in such cases no additional energy or hydrogen is needed to operate the active thermal capacitor and drive the stabilization of the temperature [20].

PCM and thermochemical reactions as thermal capacitor are both based on a reversible process: one is chemical the other is physical

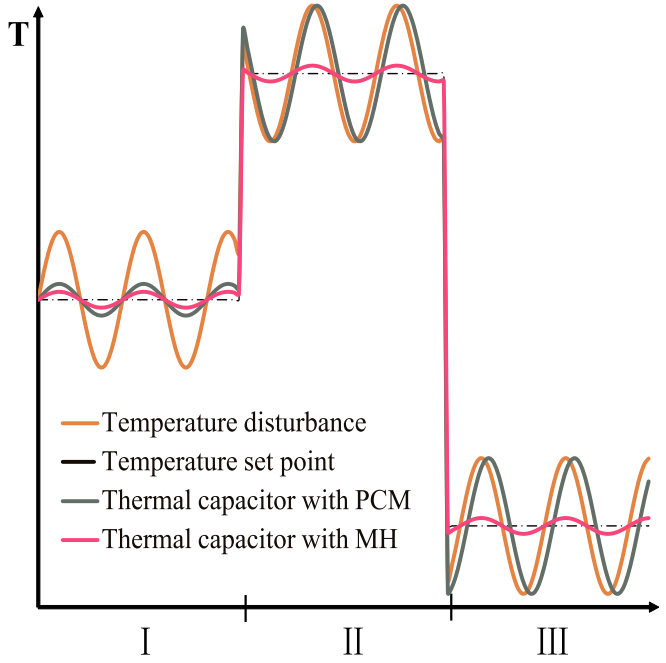

Fig. 1. Comparison PCM and thermochemical reactor for temperature stabilization [1–4].

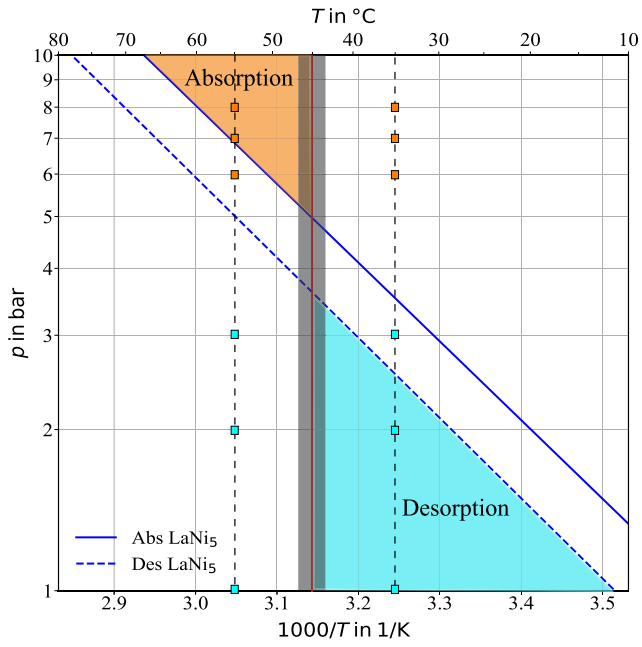

Fig. 2. Van't Hoff diagram of $LaNi_5$, including operating range of the thermal capacitor, and marked operating points for full ab-and desorption experiments.

(PCM). For heating and cooling, both systems use the respective enthalpy. While the thermal capacitor with a PCM is a passive stabilization process of the system temperature [3,21,22], the thermal capacitor with a thermochemical reactor would act as active and flexible temperature stabilization technology. To illustrate this difference, Fig. 1 compares the theoretical temperature stabilization of PCM and of the thermochemical reactor during a sinusoidal disturbance as well as the flexible adjustment to new set points. The disturbance inlet temperature is orange, the outlet temperature of a PCM thermal capacitor grey [3], the outlet temperature of thermochemical capacitor magenta, and the set point temperature grey (dashed).

In sector I the disturbance deflects around one temperature set point, which refers to the melting point of the PCM as well as to the equilibrium temperature of the TCS at the first set point pressure. During that time, the PCM and the thermochemical capacitor stabilize the temperature in a similar manner. This changes when the set point and the sinusoidal disturbance change to a higher or lower temperature as in II and III. In these cases, the latent energy of the PCM is completely consumed, thus the PCM is either completely solidified or liquid, and the remaining energy needs to be stored sensibly, therefore the temperature cannot be stabilized and follows the disturbance in orange with a small time shift due to the sensible thermal capacity of the material. In contrast, the thermochemical thermal capacitor in magenta can adjust the reaction temperature by a change of gas pressure so that it can stabilize the temperature at different set points as shown with the change of set points and disturbance in sector II and III [23]. Thus, one main advantage of the thermochemical reactor is the flexible adjustment to new temperature set points and the active control compared to the PCM.

This paper will investigate this principle based on a thermochemical reactor and a suitable 0D model of the reactor. Specific experiments with the thermochemical reactor are used to validate the model, before it is used to optimize a temperature controller. Further experiments are conducted with the optimized controller and the results are discussed. Finally, simulations with an inverted model as controller are used to investigate general limitations and dependencies between disturbance and reaction and illustrate the specific features of thermochemical capacitors.

2. Methods and model development

The discussion of the features and limitations of a thermal capacitor using a thermochemical system will be based on an experimental study in this manuscript. The reference example in this study has been defined similar to Gehring et al. [19], where temperature fluctuations in the cooling system of a fuel cell have been considered. Thus, temperature and pressure conditions are deduced from this example. However, the aim of this work is a generic view on thermal capacitors based on thermochemical systems and should not be limited to this application. This section presents first the selected material properties, then the experimental setup, first experimental results and a corresponding model validation.

2.1. Material selection

For the experiments in this study, $LaNi_5$ has been selected. It is able to reversibly react with hydrogen in a temperature range between 35 °C and 55 °C, and a hydrogen pressure range between 1 to 10 bar, which would refer to low temperature PEM fuel cell applications. With a reaction time of around 5 s, the kinetics are assumed to be faster than the heat transfer between heat transfer fluid (HTF) and material. Furthermore, a cycle stability of 45,000 cycles with a 30 % decrease in capacity and a flat plateau is considered acceptable for the application [24]. Moreover, $LaNi_5$ has a small hysteresis between ab-and desorption, which as well simplifies the regulation of the reactor to stabilize the temperature precisely. The characteristics and data of $LaNi_5$ are listed in Table 1.

Fig. 2 shows the van't Hoff diagram of $LaNi_5$.[1] The y-axis is logarithmic and shows the pressure, while the x-axis is the reciprocal temperature in Kelvin. The blue line indicates the ideal absorption equilibrium and the blue dashed graph the ideal desorption equilibrium. For the present study, it is intended that the thermal capacitor will operate between 1 bar and 10 bar. The reference temperature set point is exemplary 45 °C illustrated with a red line and the reference temperature disturbance around the set point is ± 2 K marked as grey area. The heating or the absorption reaction takes place in the pressure range of 5 bar to 10 bar and therefore with the equilibrium temperatures between 45.5 °C and 67.8 °C, which is marked in orange in the van't Hoff diagram. Whereas, the cooling or the desorption takes place in the pressure range between 1 bar and 3 bar with the equilibrium temperature between 11.7 °C and 40 °C marked in turquoise in the van't Hoff diagram. In order to characterize the system based on material and reactor, preliminary experiments for complete conversion were performed and used to calibrate the model at the temperature and pressure conditions indicated with the points in the diagram.

2.2. Experimental setup

Experiments were conducted with a 3D printed $AlSi_{10}Mg$ reactor. The reactor's design was developed in a previous work published by

Table 1
Characteristics of $LaNi_5$.

	Absorption	Desorption	Sources
Enthalpy in J/mol	28161.5	28702.3	[25]
Entropy in J mol^{-1} K^{-1}	101.74	100.78	[25]
Reaction time	5 s	3 s	Exp.
Cycle stability	45,000	45,000	[24]
Effective capacity in wt%	1.4	1.4	[26]
Plateau pressure in bar	5	5	[27]

[1] Sandia Metal Hydride database.

Bürger et. al [28], where it was used as a preheater with $LaNi_5$. Therefore, it is designed for high thermal powers showing good heat transfer properties. Fig. 3 shows the reactor on the left-hand side and the test rig with the integrated reactor on the right-hand side. The reactor consists of three tubes surrounded by a shell. Inside of the tubes a filter is located, where hydrogen flows through to the MH. The MH is inside the tube, which is equipped with fins to enhance heat transfer between MH and heat transfer fluid (HTF).

The insulated reactor is integrated into the test rig, connected with the hydrogen supply of the lab infrastructure and the thermostatic bath Lauda Proline RP890. The thermostatic bath simulates the temperature fluctuation of the inlet HTF, in which different temperature disturbances can be programmed. The volume flow of the thermostatic bath is measured by the mass flow meter DZR from Kobold Messring GmbH with an accuracy of ± 1 % and can be changed within four different levels. The insulation of the reactor decreases the heat losses to a minimum so that the assumption of no heat loss is applied. Furthermore, thermocouples of Type K with an accuracy of ± 1.5 K measure the in-and outlet temperature of the HTF and one thermocouple is supposed to be located at an axial position of 50 % of the length of the reactor in the MH material close to the filter at the center to measure the MH temperature. The temperature measurement of the MH is considered as rough indicator, but not really representative of the overall MH temperature due to the singular and not exactly known position of the thermocouple. One pressure sensor implemented in the tubes of the hydrogen supply measures the gas pressure. Two thermal mass flow meters from Bronkhorst Germany Nord GmbH (F-232MIPBD-33 V and F-111AI- 50 K-PBD-33-V) connected with the pressure sensor control the in-and outlet mass flow rate of the hydrogen with an accuracy of ± 0.5 % Rd. Due to the combination of mass flow meter, pressure sensor and control valve, they can either control the pressure or the hydrogen flow rate directly. The mass flow meters are connected to the PLC, thus an internal pressure set point can be defined manually or by an implemented controller in the PLC.

Experiments for model validation

This set up has been used for two different type of experiments for this work. First, different experiments with isothermal boundary conditions were conducted for complete ab- and desorption cycles. For these experiments, HTF temperature and gas pressure levels were varied to characterize the dynamics of the reactor in the range of operation. The HTF temperature was varied between 35 °C, 45 °C, 55 °C and the gas pressure between 1 bar to 8 bar for different experiments as marked in Fig. 2. The desorption pressures were adjusted from 1 bar to 3 bar in one bar steps and the absorption pressures from 6 bar to 8 bar in one bar steps at constant HTF temperatures for each experiment. The temperature set point was implemented in the control of the thermostatic bath. In this way, the reactor and tubes were tempered to the set temperature and held at a constant temperature for 10 min until the experiments were performed. To initiate the reaction, the pressure was manually set in the inlet flow meter and the isobaric absorption experiment took place for ~ 30 min until for at least ten minutes the hydrogen inlet flow is below 0.3 Nl/min. After complete absorption, the inlet flow meter was closed and the outlet flow meter was set to the target desorption pressure so that the isobaric desorption experiment took place for 60 min until for at least ten minutes the hydrogen outlet flow is below 0.3 Nl/min. During the whole experiment the inlet temperature of the HTF stayed constant. These experiments identify the influence of the pressure temperature correlation on the reaction dynamics and will therefore be used to validate the reactor model.

A second type of experiment was conducted with a temperature inlet disturbance of the HTF and a temperature stabilization control to prove the concept of a thermochemical system as thermal capacitor. The temperature disturbance was a theoretical sinusoidal bidirectional deflection around the temperature set point to focus on the generic concept. The amplitude and frequency of these deflections was selected to lead to a thermal energy release and intake of around 38 % of the MH capacity, thus two deflections (absorptions or desorptions) can be successively conducted. The disturbance was programmed in the thermostatic bath around the temperature set point of 45 °C for 5 min. Between the disturbances the temperature set point was set as temperature for 5 min.

2.3. Experiment results for model validation

The full ab-and desorption experiments, which have been performed first to characterize the reactor, indicate the reaction dynamics of the pressure and temperature ranges. Furthermore, the experiments show the influence of the flow meter control during the experiments. The flow meters regulate the hydrogen flow depending on the pressure set point and therefore open the valves accordingly. Control parameters and conversion calculations of the flow meters are yet unknown. Moreover, delay times between gas pressure change and valve opening and closing need to be detected.

Fig. 4 shows the experimental results for full ab- and desorptions at the ab- and desorption pressure pairs of 6 bar and 1 bar (purple), 7 bar and 2 bar (orange) and 8 bar and 3 bar (turquoise) in solid lines. The experimental results are presented in four different diagrams illustrating the MH temperature and the loading as well as the heat flow into the HTF and the thermal energy released and consumed form the MH versus time. The starts of each experimental desorption were superimposed in every diagram symbolized with the slashes in the Fig. 4.

Fig. 4a) illustrates the MH temperature of the different experiments over the time. Changing the pressure leads immediately to a change in MH temperature from the initial HTF temperature of 45 °C resulting in the temperature peaks. Maximum peaks are 50.9 °C, 51.7 °C, 55.3 °C for 6 bar, 7 bar and 8 bar during absorption. Minimum peaks during desorption are 37.8 °C, 38 °C, 39.9 °C for 1 bar, 2 bar and 3 bar during

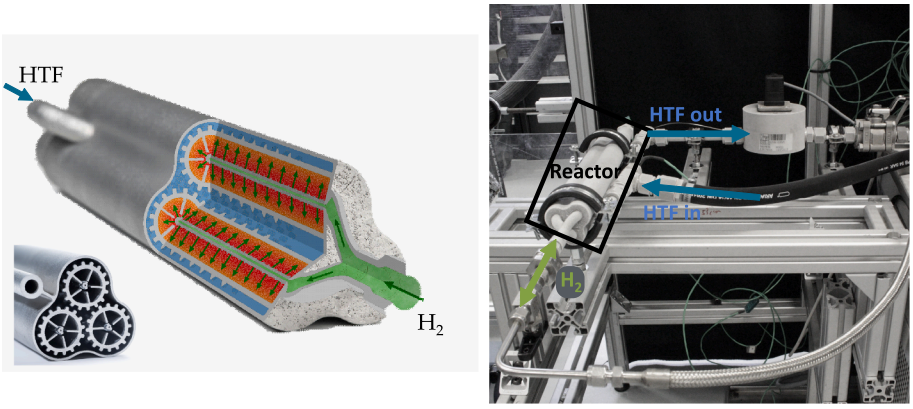

Fig. 3. Left-handed side: Reactor profile; Right-handed side: Experimental set up.

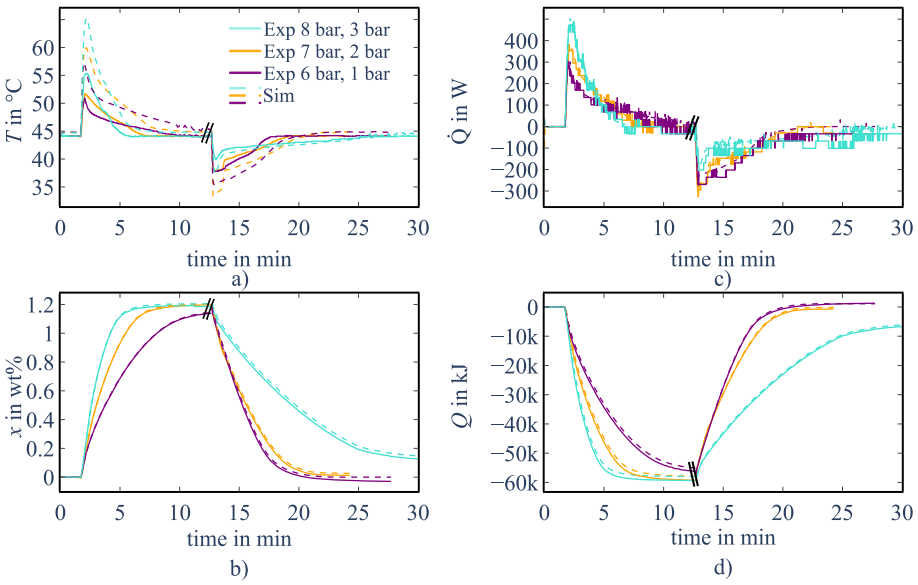

Fig. 4. Experimental (solid) and simulation (dashed) results for full ab- and desorptions at different pressures and a temperature of 45 °C: a) MH temperature, b) loading of the MH, c) heat flow between HTF and MH, d) MH reaction energy. The time for absorption has been cut to 12 min.

desorption. The experimental minimum temperature at 1 bar and 2 bar are very similar, as during the experiment with 2 bar the pressure dropped to 1 bar initially and then increased again to 2 bar, which explains as well the temperature jump during desorption up to 40.1 °C. Further values for the 2 bar desorption are therefore excluded.

The described temperature behavior is caused by the distance to the pressure temperature equilibrium. The absorption equilibrium temperatures correspond to 51 °C, 56 °C, and 60.3 °C at 6 bar, 7 bar and 8 bar, respectively. The desorption equilibrium temperatures correspond to 11.7 °C, 28.9 °C, and 40 °C at 1 bar, 2 bar and 3 bar. During absorption, the maximum MH temperatures are slightly lower than the equilibrium temperatures, while during desorption the MH temperatures are higher than the equilibrium temperatures due to the heat transfer to the HTF. Overall the experiments show the expected temperature pressure correlation of metal hydrides in a thermochemical unit: As higher/lower the pressure for ab-or desorption as higher/lower the temperature of the metal hydride and consequently as faster the reaction dynamics.

Furthermore, Fig. 4b) illustrates the loading of the metal hydride over the time illustrating the dependency of the reaction dynamics and the pressure seen in the different inclines of the graphs. The loading increases during absorption until around 1.2 wt% depending on the absorption pressure. A lower pressure results in a reduced loading (e.g. at 6 bar 1.18 wt% is reached) due to the slower reaction at lower pressures. During the desorption the loading of the MH decreases to 0 wt %.

Fig. 4c) shows the heat flow into the HTF from the MH calculated using the measured temperature difference of the in-and outlet of the HTF. An offset due to the temperature measurement and the non-perfect isothermal reactor were considered by calculating the heat losses by the temperature difference of HTF inlet and outlet during a constant inlet temperature and no reaction for five to ten minutes. During the absorption the heat flow increases first until a peak of 427.7 W at 8 bar, 354.9 W at 7 bar, and 305.2 W at 6 bar and decreases when the exothermic reaction is inhibited due to the heat accumulation, so that the reaction rate decreases. After a full absorption, the MH desorbs the hydrogen and the heat flow decreases until –269.4 W at 1 bar, and −202 W at 3 bar and rises again slowly to 0 W towards the end of the desorption experiment. This behavior shows the heating and cooling effect of absorption and desorption, respectively, and is also in accordance with the observations from temperature and conversion profiles (compare Fig. 4, a) and b)).

The thermal energy released or taken up by the metal hydride was calculated based on hydrogen conversion and the ab-or desorption enthalpy, respectively. As shown in Fig. 4d), the metal hydride released during absorption between 56 kJ and 59.3 kJ, while during desorption the metal hydride receives energy between 60.4 kJ and 54 kJ. The respective thermal energy calculated based on the metal hydride mass balance and the energy balance of the HTF differ in the absolute maximum from 2 kJ to 10 kJ depending on how much thermal energy was generated (not shown here). This indicates low thermal losses and thus a good heat transfer as well as sufficient insulation of the test bench.

2.4. Model description and validation

A mathematical model of the metal hydride reactor will be used to investigate and discuss the concept of a thermal capacitor based on a thermochemical reaction with metal hydrides. The mathematical model describes the reaction of the MH and the heat transfer between MH and HTF in the setup used for the previous experiments. It is simplified as a lumped 0D-model with only one representative tube. Three different control volumes: hydrogen gas, cooling fluid and the hollow cylinder of the MH fully define heat transfer and reaction in the reactor [19]. The assumptions for this model can be summarized as:

- Hydrogen is an ideal gas.
- The hydrogen mass flow rate of the inflow and outflow are implemented as (volumetric) source term.
- Other mass transport limitations are neglected.
- The thermodynamic equilibrium is described by van't Hoff equation and a linearization for the plateau slope.
- Thermal conductivity λ and specific heat capacity c_p, do not vary with transformed fraction, temperature or pressure.
- The reactor wall is not modeled.
- Radial and axial heat transfer in the MH is not considered in detail but summarized as part of the heat transfer resistance between MH and HTF.
- The external heat transfer coefficient is independent of the velocity of the heat transfer fluid.

The resulting relevant equations are summarized in Table 2. The energy balance for the HTF describes the change in the HTF outlet temperature $T_{HTF,\ out}$, which basically depends on the heat transfer

Table 2
Equations used for numerical model based on [19].

Reaction kinetics	$\frac{\partial x}{\partial t} = K_{Ar} e^{-\frac{E_A}{RT_{MH}}} f(p) f(\mathbf{x})$
Loading term	$f(x) = \begin{cases} x_{max} - x, Absorption \\ x, Desorption \\ 0, noreaction \end{cases}$
Pressure term	$f(p) = \begin{cases} ln\left(\frac{p_{gr}}{p_{eq}(T_{MH}, x)}\right), Absorption \\ \frac{p_{gr} - p_{eq}(T_{MH}, x)}{p_{eq}(T_{MH}, x)}, Desorption \end{cases}$
Equilibrium pressure	$f\left(p_{eq}\right) = \begin{cases} p_0 exp\left(\frac{-H_{Abs}}{RT_{MH}} + \frac{S_{Abs}}{R} + 0,2007(x - 0,5x_{max})\right), Absorption \\ p_0 exp\left(\frac{-H_{Des}}{RT_{MH}} + \frac{S_{Des}}{R} + 0,103(x - 0,5x_{max})\right), Desorption \end{cases}$
Mass balance hydrogen	$\frac{\partial p_{gr}}{\partial t} = \frac{RT_{MH}}{M_{H_2} V_V}\left(\dot{m}_{H_2} - \frac{\partial x}{\partial t}\frac{m_{MH}}{100}\right)$
Ideal gas equation	$\rho_g = \frac{pM_{H_2}}{RT_{MH}}$
Energy balance metal hydride bed	$\frac{\partial T_{MH}}{\partial t} = \frac{1}{m_{MH} c_{v,MH}}\left[-G_{th}\Delta T_{MH,HTF} + \frac{\partial x}{\partial t}\frac{m_{MH}\Delta H_R}{100 M_{H_2}}\right]$
Energy balance heat transfer fluid	$\frac{\partial T_{HTF,\,out}}{\partial t} = \frac{1}{\rho_{HTF} c_{p,HTF} V_{HTF}}\left[-G_{th}\Delta T_{MH,HTF} + \dot{m}_{HTF} c_{p,HTF}\left(T_{HTF,in} - T_{HTF,\,out}\right)\right]$
Initial conditions	$T_{MH,0} = T_{MH}(0)$; $T_{HTF,\,out,0} = T_{HTF,\,out}(0)$; $p_{gr,0} = 1$ bar; $x_0 = 0$ wt%

between HTF and MH as well as the enthalpies of the inlet and outlet flow of the HTF. Furthermore, the energy balance for the MH defines the temperature behavior of the MH and highly depends on the MH reaction rate, which depends on the Arrhenius as well as a pressure and loading term. Both pressure and loading term differ for ab- and desorption as described in Table 2. The pressure term is calculated with the equilibrium pressure p_{eq} and the gas pressure of the system p_{gr} [29–32]. However, the equilibrium pressure is calculated based on pressure-composition-temperature measurements of Willers [33] with a modified van't Hoff equation, which considers the slope of the plateau [34].

For the numerical simulation of the model, *Python* has been used with the numerical solver of *lsoda* from FORTRAN. The relative and absolute tolerance are 10^{-10} and 10^{-11} for all variables, respectively. Lower tolerances did not improve the results and only increased the computational time. The solver uses a maximum step size of 0.1 s.

The thermal conductance G_{th} was roughly calculated to 50 W/K. The Arrhenius coefficient K_{ar} was calibrated with the experimental data at 35 °C and 55 °C of the loading and the heat flow between MH and HTF, thus the optimization depends on one mass balance and one energy balance. Subsequent, the model was validated with the results of further loading and thermal energy flow of HTF experiments at 45 °C. The average R^2 for the loading is 99.9 % for the heat flow 87.7 % and 97 % depending on the experiment. This can be explained by the validation and optimization process as well as by the temperature measurement uncertainties.

Fig. 4 illustrates the validation of the model with experimental data at different ab- and desorption pressure pairs 6 bar and 1 bar in purple, 7 bar and 2 bar in orange, and 8 bar and 3 bar in turquoise at 45 °C and the simulation data in the same colors, but with dash lines. The presented results of the model were calculated with the experimental hydrogen flow as input data. The hydrogen flow defines in the calculations mainly the reaction dynamics and the heat transfer due to the reaction. Furthermore, the constant HTF inlet temperature and the mean value of the HTF flow of the experiments define the corresponding input parameters in the model. The maximum loading of the model has been set to 1.205 wt%, which is the average maximum of the loading from all experiments.

Fig. 4a) shows the model loading in the dashed lines. The curves are following the experimental results in a straight line as quantified with the R^2-value. Fig. 4b) shows the heat flow from the MH into the HTF. The K_{Ar} value of the model was well calibrated and thus it is suitable for a validation. The simulation results (dashed) follow the experimental results (straight), qualitatively and quantitatively.

In contrast, the modelled metal hydride temperature shown in Fig. 4a) differ quantitatively from the experimental data. The maximum difference between model and experiment are 10 K for 8 bar absorption and 5 K for 2 bar desorption. These discrepancies could occur due to the effect of an offset of MH temperature between model and experiment, which is 0.8 K, as well as the not considered heat loss and the inaccurate measurement. Furthermore, the thermal energy of the MH as shown in Fig. 4d) represents the potential maximum thermal energy, which can be provided to the HTF. The MH thermal energy differ 0.1–0.3 kJ from the absorbed/released thermal energy from the HTF. This indicates an almost lossless heat transfer as modeled. Moreover, again the comparison between model and experimental results are quantitatively and qualitatively accurate. Taking the results shown in Fig. 4 a)-d) into account, the model can be seen as locally validated in the temperature range of 35 – 55 °C and a pressure range of 1 bar to 8 bar.

3. Thermochemical unit as thermal capacitor

In the previous part of the manuscript, the experimental setup has been introduced and a corresponding model has been validated for rather simple charging /discharging experiments. This section is dedicated to the operation of the reactor as thermal capacitor during bidirectional disturbances in the inlet temperature of the HTF. Therefore, two different temperature controllers have been considered, which both define the required gas pressure or/and the needed hydrogen mass flow to stabilize the outlet temperature. For the first step, the validated 0D-model has been used to optimize the PID-parameters, which were then implemented in the PLC test bench. For the second step, the 0D-model was simplified and inverted to be used as feedforward controller in the simulation.

3.1. Experimental investigation and proof of concept

The first experimental attempt as a proof of concept of the thermochemical thermal capacitor is a two-loop feedback PID-controller as in Gehring et al. [19]. Fig. 5, top, a), shows a scheme of the PID- feedback controller loop. It consists of an inner and outer controlling circuit. The inner control circuit defines the accurate hydrogen flow depending on the difference between set point pressure and pressure in the reactor, while the outer circuit controls the temperature difference between set point temperature and HTF outlet temperature by indicating the set

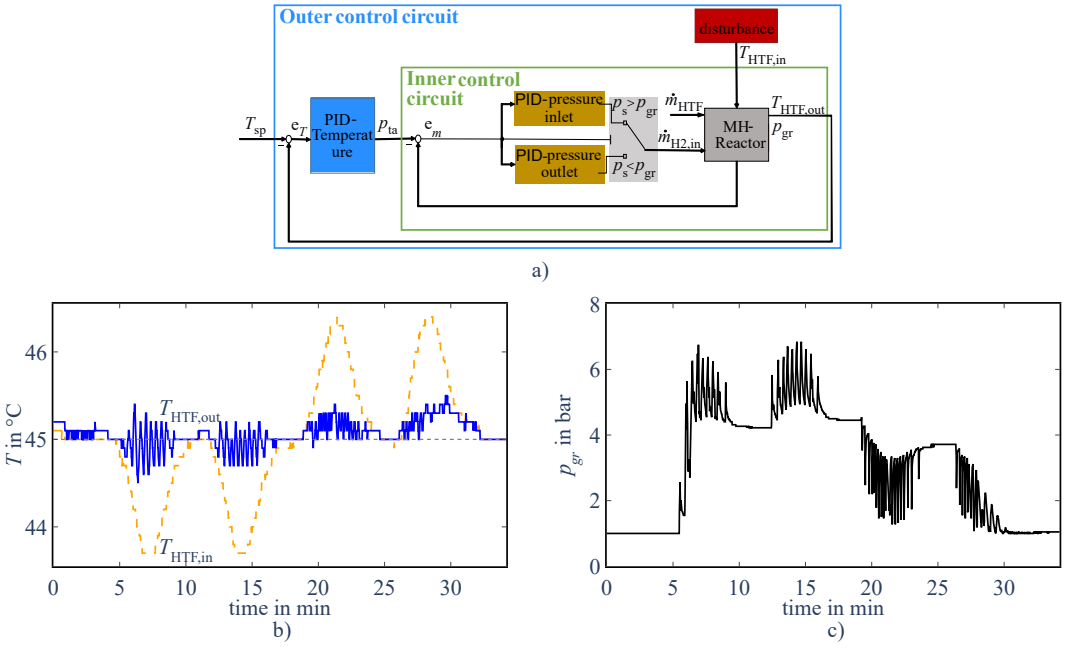

Fig. 5. a): Schematic PID-feedback controller loop for the thermal capacitor. b): temperature inlet and outlet of experimental results with the PID-controller and a disturbance of 1.5 K. c): pressure results of the experiment.

Table 3
Parameters of the optimized temperature PID-controller.

K_P	T_I	T_D	T_1	Sampling time
3.5177	63.7264	1.2008	0.25	0.5

point pressure in the reactor. The inner circuit is implemented in the test rig with two flow meters one for the inlet and one for the outlet hydrogen mass flow, symbolized in Fig. 5 with the two pressure branches, which have yet unknown controller parameters to regulate the flow or pressure. The disturbance of the system is the change of the HTF inlet temperature.

The parameters for the temperature PID-controller from the outer circuit were optimized with the model of the reactor and the inner control circuit using *MATLAB/Simulink*. The optimized parameters are listed in Table 3 for a PID-controller with delay. A PID-controller with these parameters was implemented in the PLC of the test rig to define the required gas pressure to stabilize the HTF outlet temperature and transfer it to the inner control circuit with its in-and outlet flow meters.

Fig. 5 b)/c) show the first result of the temperature stabilization with the MH reactor during a disturbance in the HTF inlet temperature of 1.5 K and an HTF volume flow of 150 l/h. Fig. 5b) shows in orange the inlet temperature, in grey (dashed) the set point temperature and in blue the outlet temperature of the HTF in °C. Fig. 5 c) shows the corresponding gas pressure in the reactor. Two identical disturbances marked in orange from the set point are consecutively applied lowering the HTF inlet temperature, afterwards two consecutive cooling scenarios of the HTF are applied. The energy required to buffer each disturbance is calculated to 22 kJ to 23 kJ depending on the thermostatic bath and corresponds to 38 % of the MH capacity. As consequence of the HTF inlet temperature disturbance to a temperature below the set point temperature, heat input is required. Thus, the controller translates this information into a gas pressure (black) increase above the equilibrium pressure, which will result in the exothermal absorption. Cooling is required during the HTF inlet temperature disturbance to a temperature above the set point temperature. Consequently, the controller changes the mode to decreasing the gas pressure in order to desorb. As shown in Fig. 5, the reaction triggered by this pressure increase for heating and decrease for cooling, enables a stabilization of the outlet temperature of the HTF (blue) around the set point of 45 °C. Thus, the experiments show an experimental proof of concept a TCS based bidirectional temperature stabilization.

Next to this general observation, two important facts can be observed from the measurements: First, the outlet temperature oscillates with peaks of up to 33.3 % from the disturbance. This behavior is an indication of an improvable controller. The control system reacts slowly compared to the reaction and the heat transfer, and cannot predict next steps. The valves controlled by the PID-controller react with a time shift of ~ 2 s after changing the set point pressure, thus real gas pressure and set point pressure differ in time.

Second, the outlet temperature rises to the inlet temperature during the last desorption showing the lack of hydrogen in the MH to provide sufficient cold to cool down the HTF accordingly. The pressure decreases to 1 bar, which is the minimum possible pressure in the setup, however, the MH does not cool the HTF anymore. This behavior is a clear indication of the MH reactor's batch behavior. Both effects, the oscillation and the batch limitation indicate the challenges a PID-controller faces with a highly nonlinear batch process. Model predictive controllers could calculate the state of charge (SoC) and use the knowledge of the reactor dynamics to reduce the challenges of controlling a highly non-

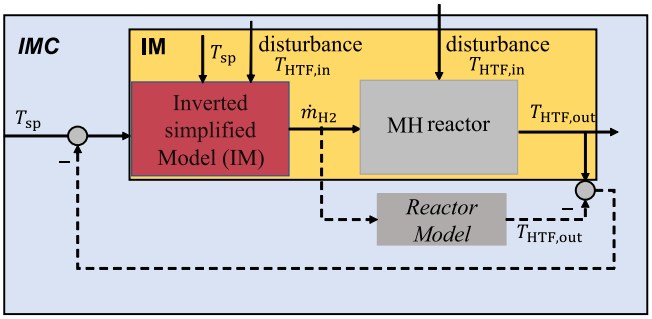

Fig. 6. Schematic of IM-system without feedback loop in yellow and IMC with feedback loop in blue. (For interpretation of the references to color in this figure legend, the reader is referred to the web version of this article.)

linear batch system. Further improvements in the details of the whole control system e.g. valves, controller and sensors are needed. Therefore, for the remaining of the manuscript another approach is followed to study the concept of a metal hydride based thermal capacitor. A simulation with an inverted model and a close to perfect controller is used to investigate the features and challenges of the concept.

3.2. Combination of inverted model and reactor model for a conceptual proof

The validated reactor model is linked with a model-based feedforward control to investigate features and challenges of the thermal capacitor. Therefore, a simplified and inverted reactor model (IM) calculates the required hydrogen mass flow to stabilize the outlet temperature depending on the inlet temperature disturbance illustrated in Fig. 6 (in yellow). This method considers the exact reactor's behavior, thus can precisely control the outlet temperature of the reactor model. The precise control can show the potential of the thermal capacitor – but, is only valid for this exact reactor. The IM is based on the idea of an internal model control (IMC) as shown in Fig. 6 marked in light blue where the inverted simplified model operates as controller and the feed backward-loop would be defined by the difference outlet temperature of the MH reactor and model. The IMC could be later on a well-suited controller for the thermal capacitor [35–37]. Therefore as first step to an improved controller, the IM was implemented as *Python* model connected with the reactor model as shown in Fig. 6 marked in yellow to simulate different scenarios of HTF volume flow, frequency and amplitude of the disturbance.

The IM is connected with the model as a controller without a feedback loop and calculates the required hydrogen mass flow for a specific temperature disturbance. This simplification of the controller is possible due to the high similarity of IM and reactor model. The IM is simplified by no implementation of the hysteresis, which leads to unavoidable deviations compared to the reactor model (compare chapter 2). As additional simplifications the equations of the model were linearized and the reaction dynamics are independent of the loading. Both simplifications lead to the equations in Table 4 (based on Table 2) and an accuracy of a R^2-value between simplified model and experiment for the loading of around 99 % and for the heat flux between HTF and MH between 85 % and 95 %.

Simulation results of the reference case:

Fig. 7 shows the simulative reference case of a thermal capacitor with MH to stabilize the HTF outlet temperature during a temperature disturbance of the HTF inlet temperature. The HTF inlet temperature disturbance is implemented in the system with a generic sinusoidal deflection. The sine curve has an amplitude of 2 K, the set point temperature is 45 °C, and a frequency of 0.0105 1/s is applied, thus one disturbance peak takes in total 5 min. An additional parameter is the HTF mass flow rate of 150 kg/s. The combination of these parameters leads to an energy requirement of 56.8 kJ to compensate the HTF inlet temperature to the set point temperature.

As introduced before, the goal of the thermal capacitor with MH is the stabilization of the HTF outlet temperature during HTF inlet temperature disturbances. In the following, the processes related to this system are introduced step by step. First, in order to compensate the disturbance, heat needs to be transferred from/to the MH to/from the HTF, thus a temperature gradient between MH and HTF is required. Therefore, the MH temperature must be adapted to the required heat transfer between HTF and MH resulting in an anticyclic behavior compared to the inlet temperature. In order to trigger this temperature behavior in the material, the gas pressure needs to be adjusted accordingly in the MH. Here the IM comes into play: It calculates the required energy to change the MH temperature depending on the difference of the set point and HTF inlet temperature leading to a required reaction rate in the MH. Next, the required gas pressure for this MH temperature is calculated with the Arrhenius equation depending on the required reaction rate. The mass balance of the hydrogen then finally defines the required hydrogen flow rate as a result of the required pressure.

Fig. 7a) illustrates the temperatures of MH as well as in and outlet of HTF versus time. As predicted, the MH temperature is anticyclic to the HTF inlet temperature disturbance. This was achieved by the pressure change in the reactor as shown in Fig. 7b). The set point pressure p_{sp} increases for heating (absorption) and decreases for cooling (desorption) and is in between the equilibrium pressure of ab-and desorption due to the simplification of the IM. During desorption the reactor pressure p_{gr} is below the desorption equilibrium pressure $p_{eq,des}$ releasing hydrogen as illustrated in Fig. 7c) reducing the loading from 1.205 wt% to 0.037 wt% and cooling the HTF. During absorption p_{gr} is above absorption equilibrium pressure $p_{eq,abs}$ taking up hydrogen as shown in Fig. 7c) increasing the loading from 0.037 wt% to 1.19 wt% and heating the HTF. This stabilizes the HTF outlet temperature as shown in Fig. 7a). The stabilized HTF outlet temperature proves the theoretical ability of the thermal capacitor to control and buffer temperature peaks.

Furthermore, the Fig. 7 shows the effects of the hysteresis and the different implementation of it in the IM and in the reactor model. First indication of the hysteresis effects is the outlet temperature deviation during the change of absorption to desorption and vice versa. The highest deviation of HTF outlet temperature and the temperature set point is 0.17 K, which refer to 8.5 % of the temperature disturbance. It is exactly located in between the hysteresis, when no ab- or desorption occur. During this time at around 5 min the equilibrium pressure stays constant due to the modelling assumptions that no reaction takes place. Furthermore, p_{gr} increases abruptly changing from desorption to absorption and jumps from 3.29 bar to 4.36 bar and increases until 8.9 bar. This pressure jump causes as well a higher p_{gr} than the p_{sp} with a maximum difference of 3.4 bar. Whereas, the pressure jump from

Table 4
Simplified and linearized equations of Table 2 based on [19].

Reaction dynamics	$\frac{\partial x}{\partial t} = K_{Ar}\left(2.7826779510^{-8}T_{MH} - 8.27176471210^{-6}\right)f(p)f(x)$
Loading term	$f(x) = \begin{cases} 1, Absorption \\ 1, Desorption \end{cases}$
Pressure term	$f(p) = \frac{p_{gr} - p_{eq}(T_{MH}, x)}{p_{eq}(T_{MH}, x)}$
Equilibrium pressure	$f\left(p_{eq}\right) = 10^5(0.1536815879T_{MH} - 44.55770548)(0.15202322532315x + 0.910008047876619)$
Mass balance hydrogen	$\frac{\partial p_{gr}}{\partial t} = \frac{RT_{MH}}{M_{H_2}V_{DV}}\left(\dot{m}_{H_2} - \frac{\partial x}{\partial t}\frac{m_{MH}}{100}\right)$
Ideal gas equation	$\rho_g = \frac{pM_{H2}}{RT}$
Energy balance metal hydride bed	$\frac{\partial T_{MH}}{\partial t} = \frac{1}{m_{MH}c_{v,MH}}\left[-G_{th}\left(T_{MH} - T_{HTF,out}\right) + \frac{\partial x}{\partial t}\frac{m_{MH}\Delta H_R}{100M_{H_2}}\right]$
Energy balance heat transfer fluid	$\frac{\partial T_{HTF,\,out}}{\partial t} = \frac{1}{\rho_{HTF}c_{p,HTF}V_{HTF}}\left[-G_{th}\left(T_{MH} - T_{HTF,out}\right) + \dot{m}_{HTF}c_{p,HTF}\left(T_{HTF,in} - T_{HTF,\,out}\right)\right] \stackrel{!}{=} 0$
Initial conditions	$T_{HTF,\,out,0} = 318.15$ K; $T_{MH,0} = 318.1$ K, $p = p_{eq}(T_{MH})$; $x_0 = 1.205$ wt%

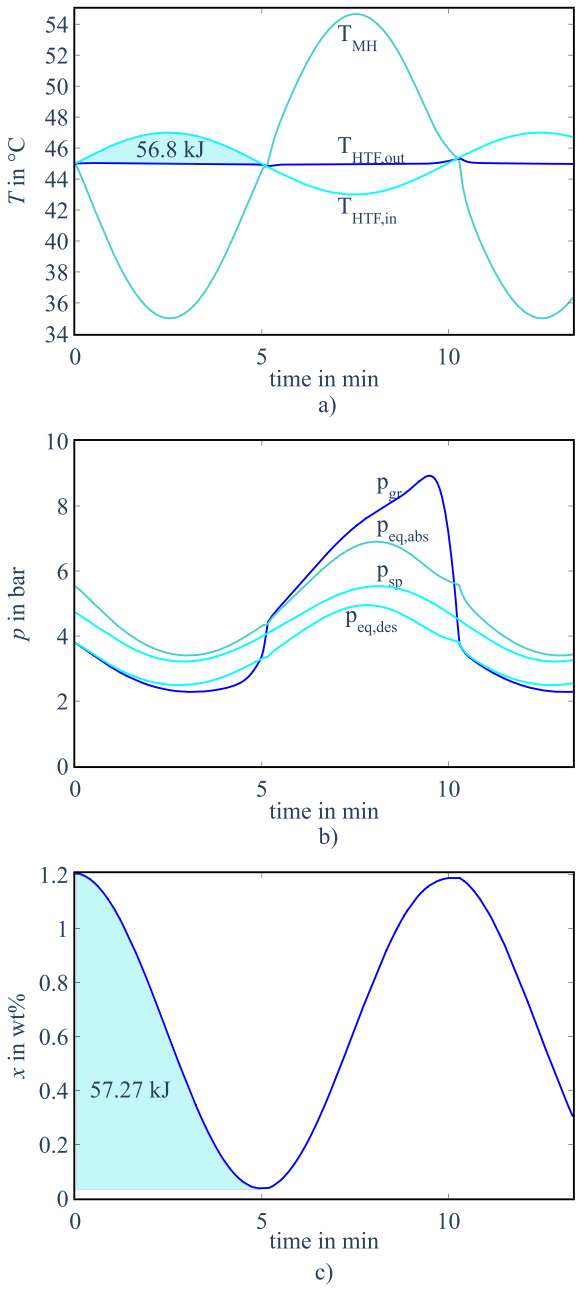

Fig. 7. Simulation of the reference case of the IM.

absorption to desorption decreases from 8.9 bar to 3.8 bar abruptly. In contrast, p_{sp} is a smooth sinusoidal curve without any jumps or interruptions laying between $p_{eq,abs}$ and $p_{eq,des}$. This difference between p_{sp} and p_{gr} as well as both pressure jumps occur due to the different implementation of the hysteresis in model and IM. The IM has no hysteresis implemented, thus the output of the IM is a smooth sinusoidal curve as the p_{sp}. In contrast, no reaction takes place between ab-and desorption in the reactor model, so that the HTF outlet temperature cannot be stabilized leading to the described deviation. This difference between the models leads to a lower absorbed hydrogen mass in the reactor model than calculated from the IM. The difference of input and uptake of hydrogen leads in the reactor model due to the small void volume to the described pressure jump changing from desorption to absorption. The pressure jump from absorption to desorption can be explained by the release of the hydrogen of the void volume while no desorption takes place.

Another discrepancy is the release and uptake of hydrogen and thus the correlated thermal MH energy calculated with the hydrogen mass balance during ab-and desorption. The MH desorbs 1.168 wt%, which takes up 57.27 kJ, while it absorbs 1.153 wt%, which releases 55.41 kJ. Thus, the thermal MH energy during desorption exceeds the required thermal energy to stabilize the temperature, while during absorption the thermal MH energy is not sufficient to stabilize the outlet temperature. The lower absorbed hydrogen mass leads to insufficient released thermal energy, which does not lead to lower HTF outlet temperature, but to an increasing outlet temperature. Meanwhile, the HTF outlet temperature as well as the MH temperature stays above the temperature set point during the hysteresis until desorption starts at an HTF inlet temperature of 45.5 °C. Other combinations frequency, amplitude and HTF volume flow could probably lead to limitations of the here proposed thermal capacitor.

3.3. Simulative results of the thermochemical capacitor's characteristics

As shown in the experiment, the thermochemical capacitor is a batch reactor with kinetic and heat transfer limitations. Further simulations with the IM and reactor model have been performed with different thermal energy consumptions or variations of frequency, of amplitude and of volume flow to demonstrate and discuss the limitations and features of this reactor and its control individually.

Temperature adjustment

One main feature of the thermochemical capacitor is the flexible adjustment of the temperature set point by changing the pressure. Fig. 8 illustrates different temperature set points and their corresponding required set pressure to achieve the temperature set point at the HTF outlet temperature. Fig. 8a) shows the inlet temperature of the HTF as disturbance with a frequency of 0.0105 1/s, an amplitude of 2 K and an

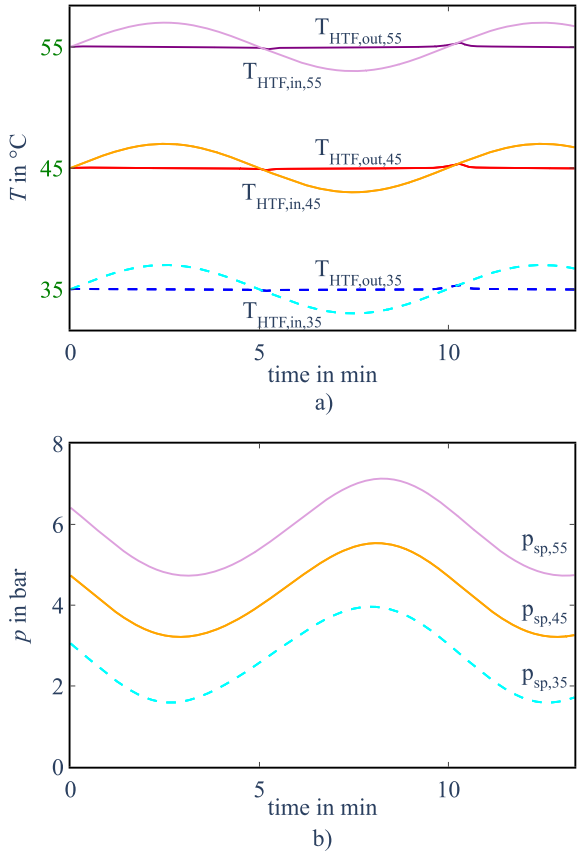

Fig. 8. Simulative results of different temperature set points at 35 °C, 45 °C and 55 °C with the IM. a) shows the HTF inlet and outlet temperature. b) shows the required set point pressure calculated by the IM.

HTF volume flow of 150 kg/s at different set points and the controlled outlet temperature of the HTF calculated by the reactor model over the time. Three different set point temperatures of 35 °C, 45 °C and 55 °C on the y-axis with green font were simulated. As intended, the HTF outlet temperatures remain constant at their set point, while the inlet temperature oscillates around the temperature set point. As a result, it is clearly shown that the temperature set point is adjustable.

Fig. 8b) illustrates the required set point pressure to control the outlet temperature at the three different temperature set points in the same color as in Fig. 8a). The three pressure graphs have the same amplitude and frequency, but oscillate around higher pressures. Comparing both diagrams, it demonstrates the direct correlation between temperature set point and pressure set point. The higher the temperature set point, the higher is the pressure set point. This correlation is related to the van't Hoff law, which defines the correlation between equilibrium pressure and equilibrium temperature of a reaction.

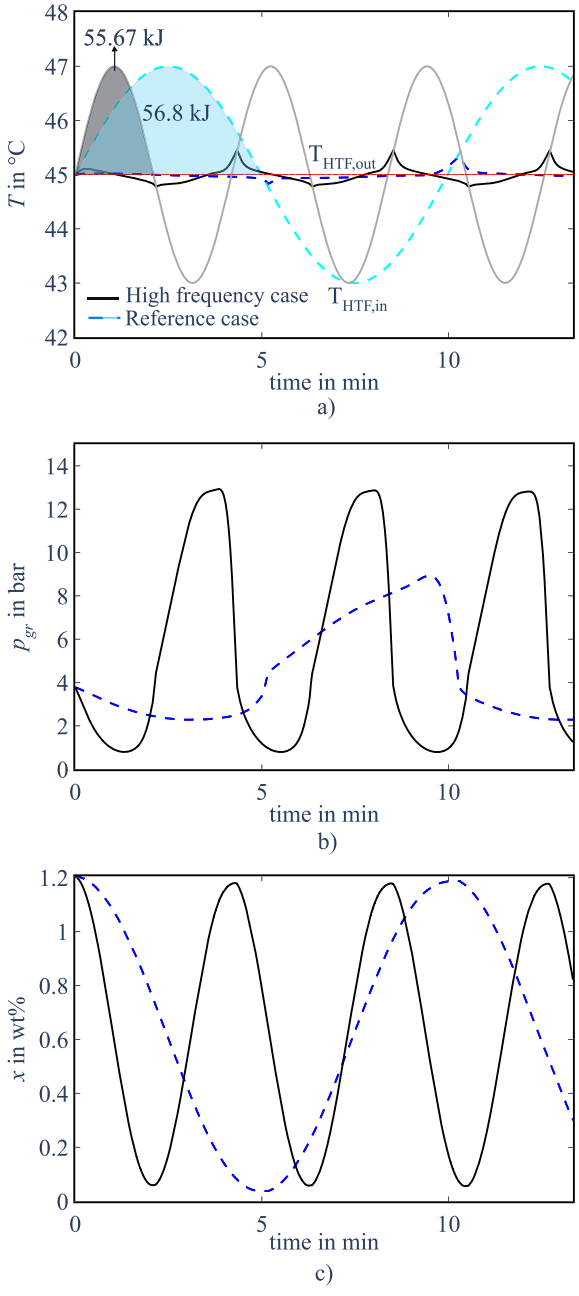

Fig. 9. Comparison of simulation results of the reference case (dashed) with a case higher frequency case needing similar thermal energy (solid). a) demonstrates the HTF in and outlet temperature, b) the gas pressure and c) the loading results.

Simulation of the dynamic effects

Another feature of the thermochemical capacitor is the influence of the reaction kinetics and thus of the temperature stabilization time. Fig. 9 shows the temperature in a), gas pressure in b) and loading in c) results of two different simulations. Both simulations have a disturbance with the same amplitude, but different volume flow of the HTF and frequency pairs 150 l/h and 0.0105 1/s (blue, dashed), and 350 l/h and 0.025 1/s (black, solid), thus leading to a similar overall thermal energy load of 56.8 kJ for the reference case and 55.67 kJ for the case with a higher frequency. Fig. 9a) shows again the resulting inlet and outlet temperature of the HTF of both scenarios versus time. The outlet temperature of the second scenario deviates maximum of 0.45 K from the set point and is 37.7 % higher than the maximum deviation of the reference scenario, but this peak only occurs once during ab-or desorption. This increase in the HTF outlet temperature peak indicates that the active control to compensate faster temperature peaks has its limitations. These limitations depend on the required thermal energy as well as the time in the hysteresis, where hydrogen does not react with the $LaNi_5$.

Fig. 9b) illustrates the gas pressure versus time. Comparing both scenarios, the scenario with the higher frequency adjusts to a higher/lower gas pressure during ab-and desorption, respectively. The higher pressure at the same temperature leads to a longer distance to the equilibrium point in the van't Hoff diagram, which accelerates the reaction and as well the regulation. Furthermore, the higher pressure leads to higher MH temperature and a faster heat transfer. This proves how the adjustment of the pressure leads to faster reaction and heat transfer regulating the HTF outlet temperature during similar thermal load, which enables an active control to buffer temperature peaks. In contrast, the PCM based thermal capacitor would show the same thermal gradient at same amplitudes and cannot actively adjust it.

Fig. 9c) demonstrates the difference of hydrogen load in the MH versus time for the two cases representing as well the different released or absorbed thermal energy of the MH. The load changes 1.15 wt% during the higher frequency and 1.16 wt% during the reference case during the first desorption. Therefore, during both cases the metal fully ab-and desorbs and the reaction dynamics are comparable.

Simulation of the batch behavior

As mentioned before, the reactor cannot continuously heat or cool the HTF, as it is a batch system. The present reactor has a maximum capacity of 1.205 wt% to store hydrogen and therefore energy, so that only a thermal energy of 57.96 kJ can be absorbed and 59.07 kJ can be desorbed in this reactor. Every required thermal energy amount, which exceeds the maximum thermal energy cannot be addressed, which causes an unstable outlet temperature of the HTF.

Fig. 10 shows one example of a batch effect with a frequency of 0.0105 1/s, an amplitude of 2.5 K and an HTF volume flow of 150 l/h in black (solid) compared with the reference case in blue (dashed). The required thermal energy exceeds the maximum providable thermal energy, thus as predicted the HTF outlet temperature rises after the thermal energy was used by fully absorbing the MH, to the HTF inlet temperature and cannot be stabilized with the reactor during the scenario with the amplitude of 2.5 K in black. The HTF outlet temperature increases up to 46.6 °C till the inlet temperature during desorption and decreases to 43.8 °C till the inlet temperature during absorption as illustrated in Fig. 10a). During absorption the hydrogen flows into the reactor while the MH is fully absorbed, so that the pressure increases rapidly as shown in Fig. 10b). The high pressure causes the maximum load of 1.205 wt% before the temperature disturbance ends. During desorption the pressure drops to the minimum limit of 0.001 bar to further trigger an endothermal desorption, but the MH is already fully desorbed. Finally, this batch effect can be seen in Fig. 10c) where the MH loading over the time of the simulation reaches 0 wt% and 1.205 wt% during desorption and absorption before the disturbance ends. This

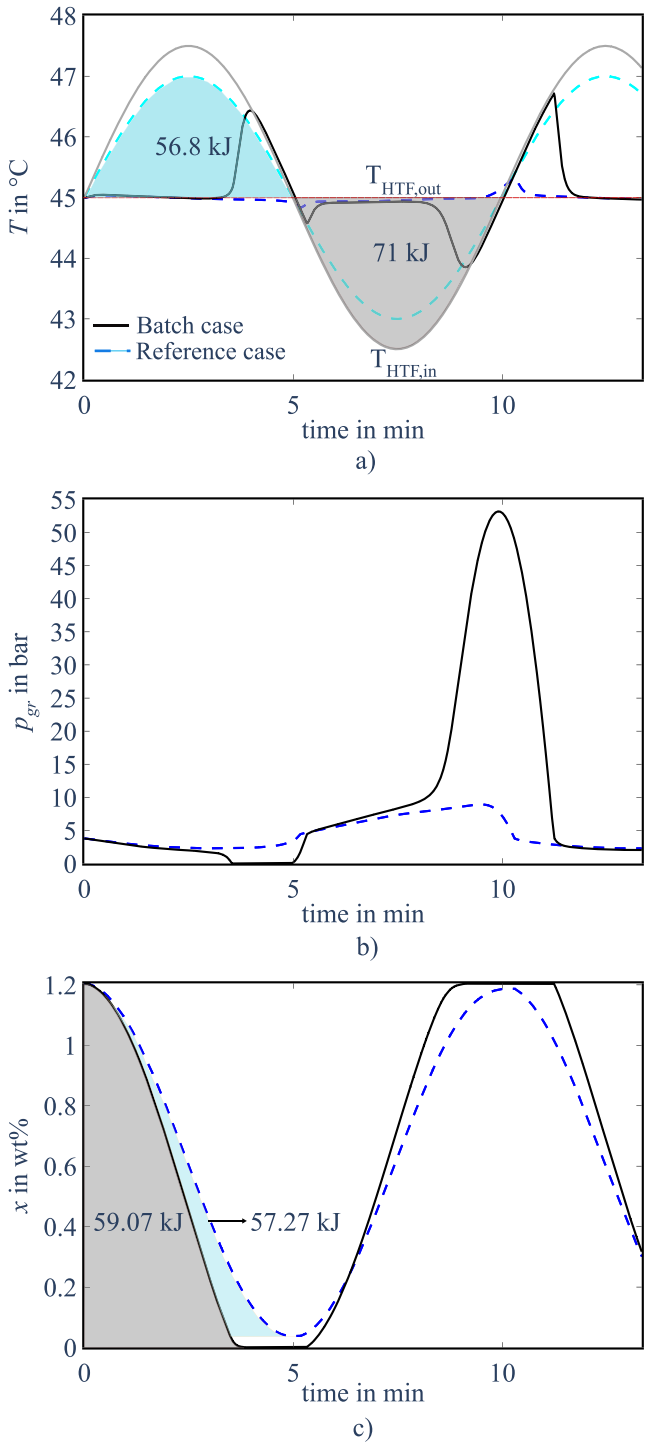

Fig. 10. Simulative comparison of reference case with a higher thermal energy case need exceeding the MH capacity. a) demonstrates the HTF in and outlet temperature, b) the gas pressure and c) the loading results.

leads to the maximal absorbed thermal energy of 59.07 kJ during desorption and the maximal released thermal energy of 57.96 kJ during absorption while the needed thermal energy to stabilize the temperature during the whole ab-and desorption time is 71 kJ. Accordingly, the required thermal energy is 20 % less than the thermal energy of the reference simulation. Hence, it would be advised to implement a SoC measurement in the controlling to regulate the batch effect and forecast upcoming limitations.

3.4. The opportunities of the IM for a thermal capacitor with MH

The thermal capacitor with MH proved in experiments its active and bidirectional temperature control. Advantageous of gas–solid reactions in comparison to the PCM is the adjustable temperature set point and reaction dynamics. The simulations with the IM show the opportunities and the flexibility as well as the challenges of the thermal capacitor indicating the wide usage in different processes and applications of the thermal capacitor with MH.

The simulations demonstrate as well the still existing problems of the thermal capacitor with MH such as the batch effect, which lead to temperature stabilization problems. One solution could be a prediction of the SoC to buffer the temperature peak for the longest time possible and not precise as possible. Another solution will be the scaling of the reactor and the reactor design for every application. A scaled reactor for every application can be achieved through scaling the size or the number of reactors. The size of the reactor can be optimized with an advanced reactor model including the reactor's geometry and the spatial gradient, while the numbers of reactors can be calculated with the current model. Moreover, the combination of IM and reactor model can lead to an easy scaling of the reactor depending on required thermal energy and temperature disturbances. Therefore, the thermal capacitor with MH can be used in small applications e.g. fuel cells or in bigger applications e.g. waste heat in steel production. A constant FC inlet temperature instead leads to less degradation than temperature deviations caused by the driving cycle. One possible solution would be, the implementation of the thermochemical capacitor into the FC's cooling circuit to stabilize the FC inlet temperature. In this case, the thermochemical capacitor would work as buffer and not as a constant cooling or heating application.

The idea of the IM as controller is based on the IMC concept. The demonstration IM shows in the combination with the reactor model a precise temperature control, which indicates the use case of an IMC as controller for the thermal capacitor. A next step to prove this concept would be the implementation of the IM in the PLC of the test rig as forward predicted control to challenge the system with real-life load cycles.

4. Conclusion

In this work, the functionality of a first-of-its-kind thermal capacitor based on thermochemical reactions was shown simulatively and experimentally. The simulation is based on a validated model of the reactor's heat transfer and reaction dynamics. This model was used to optimize a PID-controller and as underlying concept for an IM to calculate the required hydrogen mass flow. The optimized PID-controller proved the functionality of the thermal capacitor during temperature disturbances experimentally, but oscillated around the set point. Further simulations were conducted with the IM linked to the reactor model. These simulations demonstrate features and challenges of the thermal capacitor for sinusoidal temperature disturbances. The shown features are not only the dynamical and flexible response to different disturbances such as different temperature peak frequencies. Additionally, this response can be adjusted to different temperature levels by applying different gas pressures due to the thermochemical nature of the capacitor. This flexibility differentiates the thermochemical from the PCM thermal capacitor.

Nevertheless, both have the disadvantage of being a batch process with intrinsically limited thermal capacity. Therefore, one challenge will be the scaling of the reactor for different application and load scenarios. One solution to reduce the risk of the batch limitation is to apply the presented model for an online monitoring of the SoC. In such cases, the model cannot only help to optimize and scale the reactor for different applications but can also be used to optimize the respective controllers in combination with calculating the SoC. All in all, such thermal capacitor with MH could be helpful in almost all hydrogen systems, which needs a stable temperature for example fuel cells to

increase life times, industrial processes based on fluctuating renewable heat supply or chemical heat pumps to increase efficiency.

Declaration of competing interest

The authors declare that they have no known competing financial interests or personal relationships that could have appeared to influence the work reported in this paper.

Data availability

Data will be made available on request.

References

[1] F. Dal Magro, A. Meneghetti, G. Nardin, S. Savino, Enhancing energy recovery in the steel industry: Matching continuous charge with off-gas variability smoothing, Energy Convers. Manage., 104 (2015) 78–89, https://doi.org/10.1016/j.enconman.2015.05.012.

[2] M. Fong, J. Kurnia, A.P. Sasmito, Application of phase change material-based thermal capacitor in double tube heat exchanger—A numerical investigation, Energies 13 (2020) 4327, https://doi.org/10.3390/en13174327.

[3] Y. Liu, Z. Zhang, N. Zhang, Y. Yuan, P.E. Phelan, Thermal buffering performance of passive phase change material micro-pillar array systems on temperature regulation of microfluidic chips, J. Energy Storage 58 (2023) 106424, https://doi.org/10.1016/j.est.2022.106424.

[4] S. Park, D.S. Jang, D. Lee, S.H. Hong, Y. Kim, Simulation on cooling performance characteristics of a refrigerant-cooled active thermal management system for lithium ion batteries, Int. J. Heat Mass Transfer 135 (2019) 131–141, https://doi.org/10.1016/j.ijheatmasstransfer.2019.01.109.

[5] M. Jiménez-Arreola, R. Pili, F. Dal Magro, C. Wieland, S. Rajoo, A. Romagnoli, Thermal power fluctuations in waste heat to power systems: An overview on the challenges and current solutions, Appl. Therm. Eng., 134 (2018) 576–584, https://doi.org/10.1016/j.applthermaleng.2018.02.033.

[6] T. Kim, Comparative analysis on the part load performance of combined cycle plants considering design performance and power control strategy, Energy 29 (2004) 71–85, https://doi.org/10.1016/S0360-5442(03)00157-9.

[7] G. Nardin, A. Meneghetti, F. Dal Magro, N. Benedetti, PCM-based energy recovery from electric arc furnaces, Appl. Energy 136 (2014) 947–955, https://doi.org/10.1016/j.apenergy.2014.07.052.

[8] S. Mauran, H. Lahmidi, V. Goetz, Solar heating and cooling by a thermochemical process. First experiments of a prototype storing 60 kW h by a solid/gas reaction, Sol. Energy 82 (2008) 623–636, https://doi.org/10.1016/j.solener.2008.01.002.

[9] S.F. Wu, G.L. An, L.W. Wang, C. Zhang, A thermochemical heat and cold control strategy for reducing diurnal temperature variation in the desert, Sol. Energy Mater. Sol. Cells 235 (2022), https://doi.org/10.1016/j.solmat.2021.111460.

[10] E. Pahon, D. Hissel, N. Yousfi-Steiner, A review of accelerated stress tests dedicated to proton exchange membrane fuel cells – Part I: Fuel cell component level, J. Power Sources 546 (2022), https://doi.org/10.1016/j.jpowsour.2022.231895.

[11] P. Pei, H. Chen, Main factors affecting the lifetime of Proton Exchange Membrane fuel cells in vehicle applications: A review, Appl. Energy 125 (2014) 60–75, https://doi.org/10.1016/j.apenergy.2014.03.048.

[12] V.A. Sethuraman, J.W. Weidner, A.T. Haug, S. Motupally, L.V. Protsailo, Hydrogen peroxide formation rates in a PEMFC anode and cathode: Effect of humidity and temperature, J. Electrochem. Soc., 155 (2007) B50, https://doi.org/10.1149/1.2801980.

[13] G. Zhang, S.G. Kandlikar, A critical review of cooling techniques in proton exchange membrane fuel cell stacks, Int. J. Hydrog. Energy 37 (2012) 2412–2429, https://doi.org/10.1016/j.ijhydene.2011.11.010.

[14] I. Sarani, B. Xie, Z. Bao, W. Huo, X. Li, Y. Xu, B. Wang, K. Jiao, Analysis of phase change material thermal effects in large-scale proton-exchange membrane fuel cell based on open-source computational fluid dynamics, Appl. Therm. Eng., 216 (2022) 119143, https://doi.org/10.1016/j.applthermaleng.2022.119143.

[15] J. Chen, S. Kang, E. Jiaqiang, Z. Huang, K. Wei, B. Zhang, H. Zhu, Y. Deng, F. Zhang, G. Liao, Effects of different phase change material thermal management strategies on the cooling performance of the power lithium ion batteries: A review, J. Power Sources 442 (2019) 227228, https://doi.org/10.1016/j.jpowsour.2019.227228.

[16] X. Zhou, X. Xu, J. Huang, Adaptive multi-temperature control for transport and storage containers enabled by phase-change materials, Nat. Commun., 14 (2023) 5449, https://doi.org/10.1038/s41467-023-40988-2.

[17] J. Sunku Prasad, P. Muthukumar, F. Desai, D.N. Basu, M.M. Rahman, A critical review of high-temperature reversible thermochemical energy storage systems, Appl. Energy 254 (2019), https://doi.org/10.1016/j.apenergy.2019.113733.

[18] M. Wild, A. Steinfeld, Modelling of a high-temperature thermochemical storage reactor with radial flow across an annular packed bed using the CaCO3-CaO cycle as a model reaction, in: Proceedings of the ISES Solar World Congress, Santiago, Chile, 2019, pp. 4-9.

[19] D. Gehring, M. Kölbig, S. Göltz, J. Heidingsfeld, A. Rentz, O. Sawodny, M. Linder, I. Bürger, Metal hydride reactor for output temperature control, Int. J. Hydrog. Energy (2023), https://doi.org/10.1016/j.ijhydene.2023.10.045.

[20] M. Kölbig, C. Weckerle, M. Linder, I. Bürger, Review on thermal applications for metal hydrides in fuel cell vehicles: Operation modes, recent developments and crucial design aspects, Renew Sustain Energy Rev 162 (2022), https://doi.org/10.1016/j.rser.2022.112385.

[21] J. Luo, D. Zou, Y. Wang, S. Wang, L. Huang, Battery thermal management systems (BTMs) based on phase change material (PCM): A comprehensive review, Chem. Eng. J., 430 (2022) 132741, https://doi.org/10.1016/j.cej.2021.132741.

[22] A.P. Sasmito, T. Shamim, A.S. Mujumdar, Passive thermal management for PEM fuel cell stack under cold weather condition using phase change materials (PCM), Appl. Therm. Eng., 58 (2013) 615–625, https://doi.org/10.1016/j.applthermaleng.2013.04.064.

[23] J. Stengler, M. Linder, Thermal energy storage combined with a temperature boost: An underestimated feature of thermochemical systems, Appl. Energy 262 (2020), https://doi.org/10.1016/j.apenergy.2020.114530.

[24] Y. Josephy, E. Bershadsky, M. Ron, Investigation of LaNi5 after prolonged cycling, J. Less-Common Met., 172 (1991) 997–1008, https://doi.org/10.1016/S0022-5088(06)80005-6.

[25] E.W. Willers, M. Groll, A multi-hydride thermal wave device for simultaneous heating and cooling, J. Alloys Compd., (1999) 4, https://doi.org/10.1016/S0925-8388(99)00440-5.

[26] P. Muthukumar, M. Linder, R. Mertz, E. Laurien, Measurement of thermodynamic properties of some hydrogen absorbing alloys, Int. J. Hydrog. Energy 34 (2009) 1873–1879, https://doi.org/10.1016/j.ijhydene.2008.12.052.

[27] R. Nagar, S. Srivastava, S.L. Hudson, S.L. Amaya, A. Tanna, M. Sharma, R. Achayalingam, S. Sonkaria, V. Khare, S.S. Srinivasan, Recent developments in state-of-the-art hydrogen energy technologies–review of hydrogen storage materials, Sol. Compass 5 (2023) 100033, https://doi.org/10.1016/j.solcom.2023.100033.

[28] I. Bürger, V.E. Sourmelis Terzopoulos, C. Kretschmer, M. Kölbig, C. Brack, M. Linder, Lightweight reactor design by additive manufacturing for preheating applications using metal hydrides, Int. J. Hydrog. Energy 46 (2021) 28686–28699, https://doi.org/10.1016/j.ijhydene.2021.06.091.

[29] C. Briki, S. Belkhiria, M.H. Dhaou, F. Askri, A. Jemni, Dynamic study of a new design of a tanks based on metallic hydrides, Int. J. Hydrog. Energy 43 (2018) 1566–1576, https://doi.org/10.1016/j.ijhydene.2017.11.085.

[30] M. Ron, The normalized pressure dependence method for the evaluation of kinetic rates of metal hydride formation/decomposition, J. Alloys Compd., 283 (1999) 178–191, https://doi.org/10.1016/S0925-8388(98)00859-7.

[31] H. Dhaou, F. Askri, M.B. Salah, A. Jemni, S.B. Nasrallah, J. Lamloumi, Measurement and modelling of kinetics of hydrogen sorption by LaNi5 and two related pseudobinary compounds, Int. J. Hydrog. Energy 32 (2007) 576–587, https://doi.org/10.1016/j.ijhydene.2006.07.001.

[32] U. Mayer, M. Groll, W. Supper, Heat and mass transfer in metal hydride reaction beds: experimental and theoretical results, J. Less-Common Met., 131 (1987) 235–244, https://doi.org/10.1016/0022-5088(87)90523-6.

[33] E. Willers, Multi-Hydrid-Sorptionsanlage zur kombinierten Heizung und Kühlung, in: Institut für Kernenergie und Energiesysteme, Vol. Dr.-Ing, Universität Stuttgart, Stuttgart, 2002.

[34] M. Gambini, M. Manno, M. Vellini, Numerical analysis and performance assessment of metal hydride-based hydrogen storage systems, Int. J. Hydrog. Energy 33 (2008) 6178–6187, https://doi.org/10.1016/j.ijhydene.2008.08.006.

[35] W. Tan, H.J. Marquez, T. Chen, IMC design for unstable processes with time delays, J. Process Control 13 (2003) 203–213, https://doi.org/10.1016/S0959-1524(02)00058-6.

[36] R. Sarban, Y. Bar-Cohen, R.W. Jones, F. Carpi, Physical model-based internal model control of a DE actuator, in: Electroactive Polymer Actuators and Devices (EAPAD) 2011, Society for Optical Engineering 2011. Doi: 10.1117/12.880262.

[37] D.C. Psichogios, L.H. Ungar, Direct and indirect model based control using artificial neural networks, Ind. Eng. Chem. Res. 30 (1991) 2564–2573.